



ELSEVIER

Physica D 160 (2001) 79–102

PHYSICA D

[www.elsevier.com/locate/physd](http://www.elsevier.com/locate/physd)

## Parameter space analysis, pattern sensitivity and model comparison for Turing and stationary flow-distributed waves (FDS)

Razvan A. Satnoianu <sup>a,\*</sup>, Philip K. Maini <sup>a</sup>, Michael Menzinger <sup>b</sup>

<sup>a</sup> Centre for Mathematical Biology, Mathematical Institute, University of Oxford, Oxford OX1 3LB, UK

<sup>b</sup> Department of Chemistry, University of Toronto, Ont., Canada M5S 3H6

Received 5 June 2000; received in revised form 14 June 2001; accepted 14 September 2001

Communicated by A. Doelman

### Abstract

A new type of instability in coupled reaction-diffusion-advection systems is analysed in a one-dimensional domain. This instability, arising due to the combined action of flow and diffusion, creates spatially periodic stationary waves termed flow and diffusion-distributed structures (FDS). Here we show, via linear stability analysis, that FDS are predicted in a considerably wider domain and are more robust (in the parameter domain) than the classical Turing instability patterns. FDS also represent a natural extension of the recently discovered flow-distributed oscillations (FDO). Nonlinear bifurcation analysis and numerical simulations in one-dimensional spatial domains show that FDS also have much richer solution behaviour than Turing structures. In the framework presented here Turing structures can be viewed as a particular instance of FDS. We conclude that FDS should be more easily obtainable in chemical systems than Turing (and FDO) structures and that they may play a potentially important role in biological pattern formation. © 2001 Elsevier Science B.V. All rights reserved.

**Keywords:** Flow-distributed structures (FDS); Flow-distributed oscillations (FDO); Differential-flow instability (DIFI); Turing instability; Stationary space-periodic patterns; Hopf instability; Quadratic and cubic autocatalysis

### 1. Introduction

The spontaneous formation of mesoscopic patterns in far-from-equilibrium systems has in recent decades been studied intensively in reaction/diffusion (RD) systems with fast inhibitor diffusion [1,4,5,7,25]. Turing's diffusion-driven instability [1], which gives rise to stationary structures by symmetry breaking of the homogeneous reference state, is arguably the most influential model of this kind. Turing developed the theory in an attempt to explain morphogenesis, the development of shapes and forms in biology from undifferentiated tissue. Although to date no chemical has been conclusively identified as a morphogen, there do exist a number of candidates (see the books by Harrison [2] and Goodwin [3]).

Reaction-diffusion models exhibit a great variety of spatial patterns (see, for example [7,25] for a review). However, their relevance to biological systems has been criticised due to their extreme sensitivity to parameter

\* Corresponding author. Present address: Department of Mathematics, City University London, EC1V 0HB, UK. Tel.: +44-1865-280-615; fax: +44-1865-273-583.

E-mail addresses: razvansa@maths.ox.ac.uk (R.A. Satnoianu), maini@maths.ox.ac.uk (P.K. Maini).

values. Murray [8] illustrated this by linear stability analysis and showed that the parameter regime in which a number of reaction-diffusion models gave rise to diffusion-driven instability is really very small.

On the other hand, the role of flow on pattern formation has been studied only recently. A differential-flow, that is flow of activator and inhibitor species at different rates, was shown [9] to have a similar destabilising effect on the homogeneous steady state of a reaction-diffusion-advection (RDA) system as differential diffusion has in the Turing case [10]. The result of the differential-flow instability (DIFI) are periodic travelling waves.

More recently, Andresen et al. [11] (see also [12]), carried out a linear stability analysis of the RDA equations which describe the open flow of oscillating medium with fixed boundary conditions at the inflow. Their analysis predicted stationary waves even though all transport coefficients were equal. This seemed paradoxical since at the time only the Turing and Turing-like mechanisms involving fast inhibitor diffusion gave rise to stationary structures. Kaern and Menzinger [13] realised that the physical mechanism is *essentially kinematic* and they experimentally confirmed the predicted wave patterns. In the kinematic limit of sufficiently high flow rate the flow distributes the temporal oscillation, whose phase is fixed in space at the inflow boundary. Therefore, they refer to these stationary structures as *flow-distributed oscillations* or FDO. A necessary requirement for FDO is that the uniform reference state lies in the oscillatory (Hopf) domain.

At the same time Satnoianu and Menzinger [14] generalised this result to RDA systems with differential transport, i.e. with different diffusion and flow rates of the key reacting species. To distinguish the resulting waves from the FDO waves, the latter have been termed *flow-distributed structures* or FDS. The analysis of a generic reaction-diffusion-advection model led to the determination of the boundary in parameter space of the domain in which FDS patterns occur and clarified its relation to Turing and DIFI patterns. In particular, it was shown that the new FDS waves exist only for regions in parameter space that lie outside the Turing domain, and that the region where stationary Turing patterns are observed, in the absence of bulk flow, may be greatly expanded by the presence of a flow. It was found that an unstable (Hopf) reference state is not necessary for FDS to occur and that the parameter domain wherein FDS occurs extends into the region in which the reference state is stable.

In this paper we extend the analysis of [14] in two directions: first, we compare the parameter regimes in which FDS occurs with those in which Turing patterns occur, focusing on their parametric sensitivity; second, we assess the influence on FDS and Turing instabilities of the form of the nonlinearity in the kinetics. All our analysis is carried out on a one-dimensional domain. We find that FDS yield a richer class of patterns than those obtained from Turing instability, and the resultant patterns are supported in a larger parameter space. This is shown by the linear analysis and numerical simulations in Sections 2 and 3. In Section 4 we consider the nonlinear problem for the FDS where we seek to investigate the solution properties away from the primary FDS bifurcation point. In Section 5 we discuss the possible implications of our results to applications in biology. We conclude that the FDS mechanism is a robust morphogenetic mechanism which is more flexible in comparison with the classical Turing scenario. In fact we argue that the Turing patterns should be understood as a particular instance of the FDS mechanism. Therefore, we expect that the realisation of FDS waves should be quickly accessible in chemistry and we indicate a practical reaction mechanism to this end. Our results point to the ubiquity of FDS waves in nature.

## **2. A reaction-diffusion-advection system with unequal diffusion and flow rates: an ionic chemical system with combined quadratic and cubic autocatalytic step**

In [14] a differential-flow reactor was modelled by using as a prototype the action of an electric field coupled to a reacting medium with an ionic version of cubic autocatalator (or Gray–Scott (GS)) kinetics (we refer the reader to [15] for details of this model and the references therein, and [16] for more information on the effect of the electric fields). This is probably the most realistic, though relatively simple physically, differential-flow system where the

component species can attain different advection rates. The same physical model will be applied repeatedly here except that now we shall consider a variety of different kinetics laws for the governing chemistry.

Our first question relates to the difference in behaviour between the cases when the main kinetics step is either quadratic or cubic. To be specific we consider a model in which it is assumed that a precursor  $P^+$  is present in excess. To maintain electroneutrality we also require a further species  $Q^-$  to be present in the reactor at a concentration similar to that of  $P^+$ , though this species does not take part in the reaction. We assume that  $P^+$  decays at a constant rate to form the substrate  $A^+$  via



where  $p_0$  is the initial concentration of the reservoir species  $P^+$ . The substrate  $A^+$  and autocatalyst  $B^+$  subsequently react by following a linear combination of quadratic and cubic steps according to the scheme



where  $k_i$  are the constants and  $a, b$  are the concentrations of  $A^+$  and  $B^+$ , respectively.

With  $P^+$  and  $C^+$  present in excess, so that reactions (2.2) and (2.3) make only a small net contribution to the overall ionic balance, we can invoke the constant field approximation used extensively in previous models. A formal justification for this approximation is given in [16]. We take the reactor to be such that transverse variations in concentration can be ignored and to be sufficiently long for end effects to be negligible [17] so, effectively, we are considering a semi-infinite domain. This leads to the dimensionless reactor model (see [15] for the derivation of these equations and the influence of the electric field on their form)

$$\frac{\partial a}{\partial t} = \delta \frac{\partial^2 a}{\partial x^2} - \delta \phi \frac{\partial a}{\partial x} + \mu - pab - (1-p)ab^2 \quad (2.4)$$

$$\frac{\partial b}{\partial t} = \frac{\partial^2 b}{\partial x^2} - \phi \frac{\partial b}{\partial x} + pab + (1-p)ab^2 - b \quad (2.5)$$

where  $a, b, t$  and  $x$  are the dimensionless concentrations, time and distance along the reactor, respectively, with  $t > 0$  and  $0 < x < \infty$ . Here,  $\delta = D_A/D_B$  is the ratio of diffusion coefficients of substrate  $A^+$  and autocatalyst  $B^+$ , respectively, and  $\phi$  is a parameter denoting the intensity of the applied electric field (this can also be interpreted as the dimensionless drift velocity) which we use as the main bifurcation parameter. In [16] it is shown that the dimensional electric field intensity is computed according to the relation:  $E = z_B F \Sigma / R_g T$ , where  $\Sigma$  is the applied electric field strength,  $F$  the Faraday constant,  $R_g$  the universal gas constant,  $T$  the absolute temperature (supposed constant) and  $z_B$  the ionic charge of  $B$  (which is 1 in our case). Without any loss of generality we assume that  $\phi > 0$ . The parameter  $p \in [0, 1]$  measures the strength of the quadratic step against the cubic step. For  $p = 1$ , the nonlinearity in the kinetics is purely quadratic, while for  $p = 0$ , it is purely cubic. Since  $\delta$  couples the differential-diffusion and flow (through the  $\delta \phi$  term in Eq. (2.4)) it is also called the *differential transport ratio*. On putting  $\delta = 0$  in Eqs. (2.4) and (2.5) we recover the model discussed in [17,18].

Before going further it is worth commenting here on the relevance of considering the mixed-order autocatalysis kinetics given in Eqs. (2.4) and (2.5). In [19] the same mixed-order autocatalytic step was considered in the context of pure reaction-diffusion without any source terms and/or decay steps in the species kinetics. The interest there was to analyse the existence of constant speed travelling waves in such systems and in particular the dependence of the speed on the form of the autocatalytic step. A real life example where mixed-order autocatalysis was employed successfully is the iodate-arsenite reaction studied extensively in [20].

We are concerned here with the signalling problem whereby a small, constant time perturbation is imposed at the boundary  $x = 0$  for a long, but finite time ( $\tau > 0$ , say). Therefore, to close the problem (2.4) and (2.5) we specify the following boundary conditions:

$$a(0, t) = a_s + \varepsilon_1(t), \quad b(0, t) = b_s + \varepsilon_2(t) \quad (2.6)$$

for any  $t > 0$ , where

$$\varepsilon_i(t) = \begin{cases} \varepsilon_i, & \text{if } 0 \leq t \leq \tau \\ 0, & \text{otherwise} \end{cases}$$

and where  $\varepsilon_1, \varepsilon_2$  are small, ( $|\varepsilon_1|, |\varepsilon_2| \ll 1$ ) constant perturbations. Initially the system is considered to be in the uniform, unperturbed state

$$a(x, 0) = a_s, \quad b(x, 0) = b_s \quad (2.7)$$

where  $a_s$  and  $b_s$  are spatially uniform steady state values (that is, the constant solutions to Eqs. (2.4) and (2.5)) of  $a$  and  $b$ , respectively. A problem similar to (2.4)–(2.7) but with boundary condition (2.6) replaced by a periodic temporal small perturbation has been analysed for the model (2.4) and (2.5) with  $p = 0$  and  $\delta = 0$  in [18].

Problem (2.4)–(2.7) is a well posed problem for which results pertaining to local existence and uniqueness of solutions are standard [21]. The global existence of solutions and hence their uniqueness can be established by applying the results of [22].

We note that the kinetic (ODE) system ((2.4) and (2.5)) has a (spatially uniform) steady state

$$S = \left\{ (a_s, b_s) = \left( \frac{1}{\mu + p - p\mu}, \mu \right) \right\}$$

which exists for all  $0 \leq p \leq 1$ . A standard local stability analysis for  $S$  shows that, for given  $p$  in this range,  $S$  is stable for all

$$\mu \geq \mu_0(p) = \max \left\{ 0, \frac{\sqrt{1-p} - p}{1-p} \right\} \geq 0$$

and undergoes a Hopf bifurcation in a domain included in

$$\left\{ 0 \leq \mu \leq \mu_0(p), 0 \leq p \leq \frac{\sqrt{5}-1}{2} \right\}$$

In particular  $S$  is stable for any  $\mu > 0$  if  $p = 1$  (pure quadratic case) and  $\mu_0(0) = 1$  (corresponding to the pure cubic case). In fact the case of pure cubic autocatalysis was analysed in great detail in the literature (for example [23,24]). From these studies it is known that for  $p = 0$ ,  $S$  is stable for  $\mu > 1$  and undergoes a supercritical Hopf bifurcation at  $\mu = 1$ . This leads to stable limit cycles in the interval  $\mu_1 < \mu < 1$  ( $\mu_1 \cong 0.9003$ ). For  $\mu < \mu_1$  the kinetic system does not have a long time steady state with  $a \sim \mu t, b \rightarrow 0$  as  $t \rightarrow \infty$ .

Apart from the linear interpolation between cubic and quadratic steps considered above there are obviously other ways to combine such steps, at least at this theoretical, speculative stage. Because of this arising complexity we would like to begin in the next section with the most general situation and to return to the particular case given by system ((2.4) and (2.5)) later. In doing so we shall be able to obtain the necessary and sufficient conditions for FDS instability for any given type of nonlinearity in the kinetics (ODE) system accompanying a reaction-diffusion-advection system of the form in (2.4) and (2.5). These conditions will be illustrated below in a series of applications through a variety of kinetics schemes/nonlinear models including some widely used in the mathematical modelling of biological systems [7].

### 3. The FDS primary instability

#### 3.1. Linear analysis for pattern instability in a general reaction-diffusion-advection system

##### 3.1.1. FDS instability

In the following we shall continue to use the notation  $S$  for a generic (spatially uniform) steady state solution to a system like (2.4) and (2.5) but with general kinetics terms. To be specific the form we consider is the following:

$$\frac{\partial a}{\partial t} = \delta \frac{\partial^2 a}{\partial x^2} - \delta \phi \frac{\partial a}{\partial x} + f(a, b) \quad (3.1)$$

$$\frac{\partial b}{\partial t} = \frac{\partial^2 b}{\partial x^2} - \phi \frac{\partial b}{\partial x} + g(a, b) \quad (3.2)$$

We assume that the nonlinear functions  $f$  and  $g$  are such that the results for global existence of the solutions derived in [22] can be applied. In particular these require that  $f$  and  $g$  are Lipschitz continuous functions in the variables  $a, b$  and that there is some control for the growth parts of  $f$  and  $g$  as functions of  $a$  and  $b$ . All these requirements are usually satisfied in practice and are easy to check for the model examples used in Section 3.2 to illustrate the theory. Whenever this is the case we note that the reaction-diffusion-advection system ((3.1) and (3.2)) is the most realistic and still general set-up which gives rise to possible spatial and/or spatio-temporal instabilities such as Turing [1], DIFI [9] and/or FDS [14]. Our goal here is to establish the necessary conditions on the form of the nonlinear functions  $f$  and  $g$  which promote FDS.

Previous studies on the FDO instability [11] have claimed (without proof) that a necessary kinetic condition for the appearance of the FDO instability as a primary bifurcation from the steady state is that  $S$  should lie in the Hopf (oscillatory) instability regime. As we deal here with a more general case the situation is more complicated.

As usual, the stability of  $S$  is determined by analysing the behaviour of the linearised system around  $S$ . To do this we set

$$a = a_s + A, \quad b = b_s + B \quad (3.3)$$

where  $|A| \ll a, |B| \ll b$ . Substituting Eq. (3.3) into Eqs. (3.1) and (3.2) we obtain, after linearising,

$$\frac{\partial A}{\partial t} = \delta \frac{\partial^2 A}{\partial x^2} - \delta \phi \frac{\partial A}{\partial x} + a_{11}A + a_{12}B \quad (3.4)$$

$$\frac{\partial B}{\partial t} = \frac{\partial^2 B}{\partial x^2} - \phi \frac{\partial B}{\partial x} + a_{21}A + a_{22}B \quad (3.5)$$

subject to the boundary conditions

$$A(0, t) = \varepsilon_1(t), \quad B(0, t) = \varepsilon_2(t) \quad (3.6)$$

where

$$a_{11} = \frac{\partial f}{\partial a}, \quad a_{12} = \frac{\partial f}{\partial b}, \quad a_{21} = \frac{\partial g}{\partial a}, \quad a_{22} = \frac{\partial g}{\partial b}$$

evaluated at  $S$ .

Here we assume that the perturbation is applied at the inflow boundary  $x = 0$  for a long but finite time. This allows us to take the boundary perturbation data with time-compact support (and to be extended, if necessary, by

periodicity to the whole of  $R$ ). Therefore, the conditions of the Fourier theorem are met and we seek the general solution to Eqs. (3.4) and (3.5) as a superposition of normal modes

$$(A, B) = \int_{-\infty}^{\infty} (A_0(\omega), B_0(\omega)) e^{i\omega t + k(\omega)x} d\omega \quad (3.7)$$

From our assumptions it follows that the functions  $A_0(\omega), B_0(\omega)$  (in Eq. (3.7)) are analytic functions in the complex  $\omega$ -plane. By the inverse Fourier transform from Eqs. (3.6) and (3.7) we have

$$A_0(\omega) = \frac{1}{2\pi} \int_0^{\infty} \varepsilon_1(t) e^{-i\omega t} dt, \quad B_0(\omega) = \frac{1}{2\pi} \int_0^{\infty} \varepsilon_2(t) e^{-i\omega t} dt \quad (3.8)$$

Expression (3.7) is a solution provided  $\omega$  and  $k$  satisfy the quadratic dispersion relation in  $\omega$ :

$$\begin{aligned} D(\omega, k) = & \omega^2 + i((1+\delta)k^2 - (1+\delta)k\phi + \text{Tr})\omega - \delta k^4 + 2\delta\phi k^3 - (a_{11} + \delta a_{22} + \delta\phi^2)k^2 \\ & + (a_{11} + \delta a_{22})\phi k - \Delta = 0 \end{aligned} \quad (3.9)$$

where

$$\text{Tr} = a_{11} + a_{22}, \quad \Delta = a_{11}a_{22} - a_{12}a_{21} \quad (3.10)$$

Since we are interested in stationary-space periodic solutions (i.e.  $\omega = 0$ ) we require the coefficient of  $\omega^0$  in the dispersion relation (i.e. the free term in the quadratic in  $\omega$  in Eq. (3.9)) to be zero at the bifurcation boundary giving (see [14] for full details)

$$R \equiv \delta k^4 - 2\delta\phi k^3 + (a_{11} + \delta a_{22} + \delta\phi^2)k^2 - \phi(a_{11} + \delta a_{22})k + a_{11}a_{22} - a_{12}a_{21} = 0 \quad (3.11)$$

Solutions that bifurcate to space-periodic structures will have purely imaginary wave numbers  $k_c = iz_c, z_c > 0$ . A short calculation reveals that

$$z_c = \sqrt{\frac{a_{11} + \delta a_{22}}{2\delta}} > 0 \quad (3.12)$$

It is instructive to note that the critical FDS wave number at Eq. (3.12) coincides with the critical wave number of the Turing theory [7]. In fact at criticality we obtain three possible wave numbers given by 0 (corresponding to the uniform steady state  $S$ ) and  $\pm iz_c$  (corresponding to the bifurcating FDS solutions). This is the signature of a typical pitchfork bifurcation with the FDS bifurcation behaving similarly to the Turing bifurcation. Note that this bifurcation can only exist when  $\delta > -(a_{11}/a_{22})$ . Putting this value of  $k$  into Eq. (3.11) gives the *neutral curve of the boundary-forcing problem*, i.e. the curve  $\phi^* = \phi(\delta, f, g)$  that corresponds to the *bifurcation to stationary (FDS) solutions*:

$$\phi^{*2} = (\phi^*(\delta, f, g))^2 = -\frac{1}{2} \frac{(a_{11} + \delta a_{22})^2 - 4\delta(a_{11}a_{22} - a_{12}a_{21})}{\delta(a_{11} + \delta a_{22})} \quad (3.13)$$

for  $\delta \neq 0$  and  $a_{11} + \delta a_{22} \neq 0$ . We remark here that there is no such instability associated with the steady state solution of a single, scalar equation (i.e. we require at least two species for the instability to occur).

We can compute explicitly the eigenvalues by straightforward but involved algebra. Defining  $s_1 = \delta k^4 + (a_{11} + a_{22}\delta + \delta\phi^2)k^2 + \Delta$ ,  $r_1 = -\text{Tr} - (1+\delta)k^2$ ,  $s_2 = 2\delta\phi k^3 i + k\phi(a_{11} + \delta a_{22})i$ ,  $r_2 = -i(1+\delta)k\phi$ ,  $\alpha = r_1 r_2 - 2s_2$ ,  $\beta = r_1^2 - r_2^2 - 4s_1$ ,

$$\lambda = \frac{\sqrt{\beta + \sqrt{\beta^2 + 4\alpha^2}}}{\sqrt{2}}, \quad \eta = \frac{\alpha\sqrt{2}}{\sqrt{\beta + \sqrt{\beta^2 + 4\alpha^2}}}$$

it is easy to see, from Eqs. (3.9) and (3.10), that the eigenvalues are  $\omega^\pm = (1/2)(-r_1 \pm \lambda - i(r_2 \pm \eta))$ . In particular, when  $\phi = \phi^*$ , we have that  $\text{Re}(\omega^+) = \text{Im}(\omega^+) = 0$  at  $k = k_c$  defining the critical boundary for the FDS bifurcation to stationary solutions. Furthermore, calculations for the model kinetics systems used to illustrate the present theory in Section 3.3, show that  $(d\text{Re}(\omega^+)/d\phi)(\phi^*) > 0$  when all the other parameters are kept fixed. This shows that the FDS bifurcation is expected to occur in the region  $\phi \geq \phi^*$  in generic cases (i.e. a supercritical bifurcation). This is therefore similar to the case of a Turing bifurcation (the latter occurs in the domain  $\delta \geq \delta_T$  with  $\delta_T$  defined in Eq. (3.24)).

Now we look in more detail at expression (3.13). We have two cases to consider:

$$1 \quad (a_{11} + \delta a_{22})^2 - 4\delta(a_{11}a_{22} - a_{12}a_{21}) > 0 \quad \text{and} \quad a_{11} + \delta a_{22} < 0 \quad (3.14)$$

$$2 \quad (a_{11} + \delta a_{22})^2 - 4\delta(a_{11}a_{22} - a_{12}a_{21}) < 0 \quad \text{and} \quad a_{11} + \delta a_{22} > 0 \quad (3.15)$$

Case 1 is actually impossible since it contradicts the condition that  $z_c$  in Eq. (3.12) is real. Case 2 can only hold if  $\Delta = a_{11}a_{22} - a_{12}a_{21} > 0$ . This leads to two subcases to analyse:

2.1  $\text{Tr} = a_{11} + a_{22} < 0$ . This corresponds to  $S$  being linearly stable for the associated spatially homogeneous ODE system to (3.1) and (3.2). Without restriction suppose then that  $a_{11} < 0, a_{22} > 0$ . This corresponds to the so-called activator–inhibitor local type dynamics in the ODE system. From the second condition in (2) we require that  $\delta > 1$ . In this case the first condition in (2) implies that  $\delta$  lies between the two roots of the quadratic:

$$(a_{11} + \delta a_{22})^2 - 4\delta(a_{11}a_{22} - a_{12}a_{21}) = 0 \quad (3.16)$$

Eq. (3.16) actually corresponds to the case  $\phi = 0$  in Eq. (3.11) with the subsequent requirement that the resulting quadratic in  $k^2$  has a double root (Turing instability). Consequently we see from Eq. (3.16) that this is possible only when the discriminant

$$\Delta_\delta = -16a_{12}a_{21}\Delta \geq 0 \quad (3.17)$$

Because  $\Delta > 0$  from our assumption we see from Eq. (3.17) that the cross-diagonal terms in the Jacobian must have opposite signs. This then leads to the two possible types of kinetic interactions, namely pure activator–inhibitor and cross activator–inhibitor [7,8]. These are the only two types of nonlinear structure able to sustain the Turing instability. However, we note that in our case the parameter space for FDS instability is disjoint from the Turing domain. Let  $\delta_1 \leq \delta_2$  be the two (real) roots of Eq. (3.16). With conditions (3.16) and (3.17) satisfied we then have the condition for the spatial FDS instability (condition of the diffusion ratio and flow rates):

$$\max \left\{ 1, \delta_1, -\frac{a_{11}}{a_{22}} \right\} \leq \delta \leq \delta_2 \quad (3.18)$$

$$\phi \geq \phi^* \quad (3.19)$$

where  $\phi^* = \phi^*(\delta, f, g)$  was given in Eq. (3.13). Condition (3.19) is equivalent to the requirement that Eq. (3.11) with conditions (3.15), (3.17) and (3.18) has a solution with  $\text{Re}(\omega) \geq 0$  and  $\text{Im}(k) > 0$  giving spatial instability (see the discussion in the paragraph following Eq. (3.13)). Of course, it may be possible to have a subcritical bifurcation at  $\phi = \phi^*$  but this cannot be determined by linear analysis. In fact, using weakly nonlinear analysis, we find that for the pure cubic model this is possible (full details will be presented elsewhere [37]). We note that condition (3.19) is satisfied in all the calculations presented below for all the different kinetics schemes used.

2.2  $\text{Tr} = a_{11} + a_{22} \geq 0$ . In this case  $S$  is temporally unstable. In generic cases the condition  $\text{Tr} = 0$  corresponds to a locus for a Hopf bifurcation so that the homogeneous steady state undergoes an oscillatory motion in

the absence of any spatial instabilities. From Eq. (3.15) we still require Eq. (3.17) to be satisfied, i.e. the cross-diagonal elements of the Jacobian must have opposite signs. If all these restrictions are satisfied then FDS instability is possible. We shall require again that

$$\max \left\{ \delta_1, -\frac{a_{11}}{a_{22}} \right\} \leq \delta \leq \delta_2 \quad (3.20)$$

$$\phi \geq \phi^* \quad (3.21)$$

for  $S$  to be linearly unstable to spatial perturbations leading to FDS. Condition (3.21) is established in the same way as for Eq. (3.19). A surprising consequence of this case is the possibility of FDS being promoted even if the ODE system associated with (3.1) and (3.2) does not have an activator–inhibitor structure. This is so whenever  $a_{11}$  and  $a_{22}$  have the same sign (either positive or negative). We also note that this subcase allows for situations when  $\delta \leq$  and/or  $> 1$  which is in marked contrast to the similar conditions for a Turing bifurcation [7,8]. However, in order to make a fair comparison between the Turing and the FDS spatial instability mechanisms it is clear that one needs to extend the Turing case to allow for spatial patterning even when, initially, the uniform steady state of the system is temporally unstable. This is what we do now.

### 3.1.2. Turing instability

We define an *extended Turing bifurcation* as a bifurcation to stationary space periodic solutions in a coupled RD system from a spatially homogeneous reference state (which may be temporally stable or unstable).

To analyse the extended Turing bifurcation appropriate boundary conditions must be augmented to the system depending on the geometry and the spatial configuration of the system. Here, we analyse the extended Turing bifurcation for system ((3.1) and (3.2)) with the same boundary and initial conditions as for the previous case but with  $\phi = 0$ . The analysis is entirely similar to that for FDS so we only summarise the results. The stability of the steady state  $S$  is again determined by analysing the Eqs. (3.4) and (3.5) but now with  $\phi = 0$ . For these conditions in exactly the same manner as for the FDS case the linear solutions are given by

$$(A, B) = \int_{-\infty}^{\infty} (A_1(\omega), B_1(\omega)) e^{i\omega t + k(\omega)x} d\omega \quad (3.22)$$

where

$$A_1(\omega) = \frac{1}{2\pi} \int_0^{\infty} \eta_1(t) e^{-i\omega t} dt, \quad B_1(\omega) = \frac{1}{2\pi} \int_0^{\infty} \eta_2(t) e^{-i\omega t} dt$$

and where  $\eta_i$  are small, smooth, compact supported functions in  $0 \leq t < \infty$ . Following the standard pattern of analysis as for the FDS above we deduce from Eq. (3.22) the required dispersion relation. As before we are looking for stationary solutions so again we set the coefficient of  $\omega^0$  in the dispersion relation to zero to obtain:

$$T \equiv \delta k^4 - (a_{11} + \delta a_{22})k^2 + \Delta = 0 \quad (3.23)$$

From Eq. (3.23) the neutral curve for instability is

$$\delta_T = \delta_T(k^2) = \frac{a_{11}k^2 - \Delta}{k^2(k^2 - a_{22})} \quad (3.24)$$

whose minimum

$$k_T = \sqrt{\frac{a_{11} + \delta a_{22}}{2\delta}} > 0 \quad (3.25)$$

is the same value as in the FDS case. The neutral stability condition gives from Eq. (3.23) that  $4\delta_T \Delta = (a_{11} + \delta_T a_{22})^2 > 0$ . Thus,  $\Delta > 0$ . Note that  $\delta_T = \delta_2$ , the larger root in Eq. (3.16). From Eq. (3.25) we also have that at least one of the main diagonal terms in the Jacobian matrix is positive.

Considering first the case of bifurcation from a stable uniform steady state we have the condition that  $\text{Tr} = a_{11} + a_{22} < 0$ . Therefore, from Eq. (3.25) we have two cases to analyse:

- 1  $a_{22} > 0$ : From  $\text{Tr} = a_{11} + a_{22} < 0$  it follows that  $a_{11} < 0$ . From  $\Delta > 0$  we then have  $a_{12}a_{21} < 0$ . This is the classical activator/inhibitor type of dynamics discussed at length in [7].
- 2  $a_{22} < 0$ : From Eq. (3.25)  $a_{11} > 0$ . Again we require that the cross diagonal elements in the Jacobian must have opposite signs.

In order to aid the comparison with the FDS case we need to discuss the possible bifurcation to spatial patterns when the uniform steady state  $S$  is temporally unstable. In this case,

$$\text{Tr} = a_{11} + a_{22} > 0 \quad (3.26)$$

From Eqs. (3.24) and (3.26) we see that in this case the instability is possible with  $\delta < 1$ , for example with  $a_{22} > 0 > a_{11}$  and  $a_{22} > |a_{11}|$ . It can also hold when  $\min\{a_{11}, a_{22}\} > 0$ . This is therefore similar to the FDS case (2.2) above. Finally we remark that an extended Turing bifurcation is possible with no differential diffusion present ( $\delta = 1$ ). From Eq. (3.25) this necessarily requires that  $\text{Tr} = a_{11} + a_{22} > 0$ , i.e. the uniform reference state  $S$  is unstable.

To summarise, we have shown that classical or extended Turing and FDS instabilities are possible when  $S$  is either stable or unstable. In the former case the conditions for the FDS are given by Eqs. (3.18) and (3.19) and the condition for Turing instability is given by  $\delta \geq \delta_2$  with  $\delta_2$  being defined as the larger root of Eq. (3.16) (see [7]). In the latter case we have conditions (3.20) and (3.21) for FDS, with the same condition  $\delta \geq \delta_2$  for the Turing instability. In this latter case both instabilities can occur with  $\delta < 1$  and the activator–inhibitor structure is no longer necessary.

The stability analysis for FDS shows that  $\phi^* = 0 \Leftrightarrow (a_{11} + \delta a_{22})^2 - 4\delta\Delta \geq 0$ . We can interpret this in two ways, namely for parameter values inside the (extended) Turing domain we can either have no FDS instability or FDS coinciding with the (extended) Turing instability. The latter formulation is what we prefer as then the classical Turing patterns can be truly seen as a particular FDS solution. In this way, we can say that there is one general patterning process due to the combined action of diffusion, flow and local kinetics, which produces patterns that we propose to call *flow and diffusion distributed structures*. Therefore, the same nomenclature *FDS* is operable but under this more general understanding.

We also note that relation (3.13), for the critical neutral curve, can be arranged in a different way. We see from Eq. (3.13) that for given values of the kinetics parameters and a given flow rate there is a range of values for the diffusion ratio  $\delta$ :  $\delta_{\phi,f,g}^1 \leq \delta \leq \delta_{\phi,f,g}^2$  such that inside this interval linear analysis predicts FDS instability. For the corresponding classical Turing case we need to satisfy  $\delta \geq \delta_2$ . We have that  $\delta_{0,f,g}^2 = \delta_2$ . Therefore, for the case when  $S$  is stable (which is the case with applications in morphogenesis), the FDS instability improves considerably one of the main requirements in the Turing scenario [7], namely that the ratio of the diffusivities  $\delta > \delta_2 \geq 1$ . As it is known, for the latter it is found that the difference is a few orders of magnitude making this stringent assumption a major handicap for practical applications of the Turing theory. By contrast in the FDS case the minimum diffusion value is controlled via Eq. (3.18) by the ratio  $-a_{11}/a_{22} > 1$ . From Eq. (3.18) this not only is a smaller value than the Turing minimum value  $\delta_2$  but is also of simpler structure and easier to control.

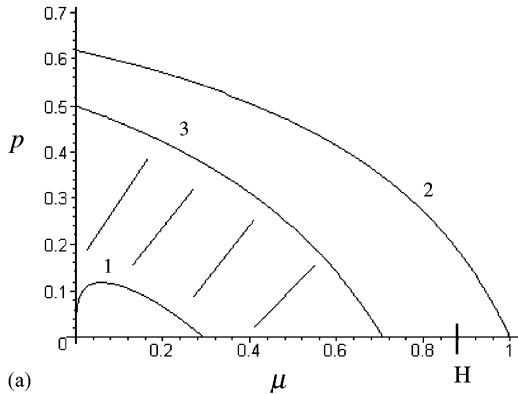
### 3.2. Illustrations

We explore now the consequences of the above theory for a variety of kinetics models. The goal is to determine the domains in parameter space where FDS and/or Turing structures occur for a set of widely employed kinetics models. We aim to find which particular nonlinearity generates spatial patterns in a robust manner and thus can be chosen as a likely candidate to guide the experimental realisation of the FDS patterns. In particular, the analysis below shows that pure quadratic nonlinearity does not promote spatial patterning.

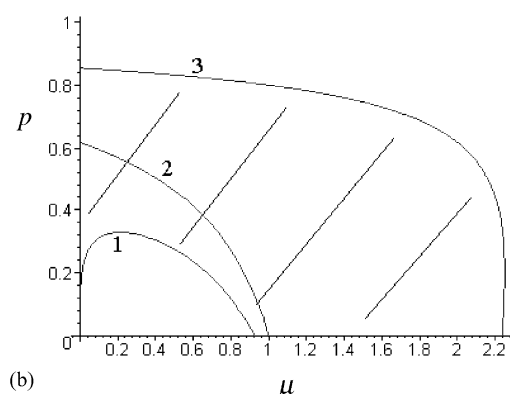
### 3.2.1. Quadratic–cubic linear interpolation model (2.4) and (2.5)

The model (2.4) and (2.5) has a generic substrate-activator type kinetics given by  $f(a, b) = \mu - pab - (1-p)ab^2$ ,  $g = pab + (1-p)ab^2 - b$ . Its uniform steady-state solution is

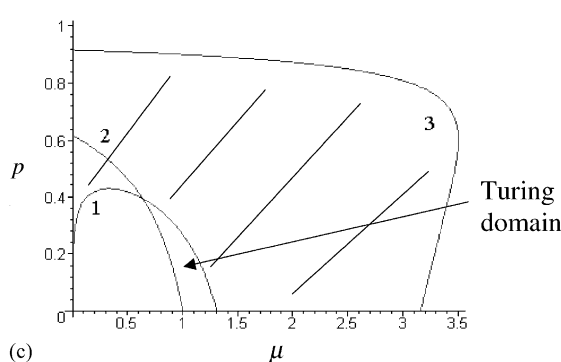
$$S = \left\{ (a_s, b_s) = \left( \frac{1}{\mu + p - p\mu}, \mu \right) \right\}$$



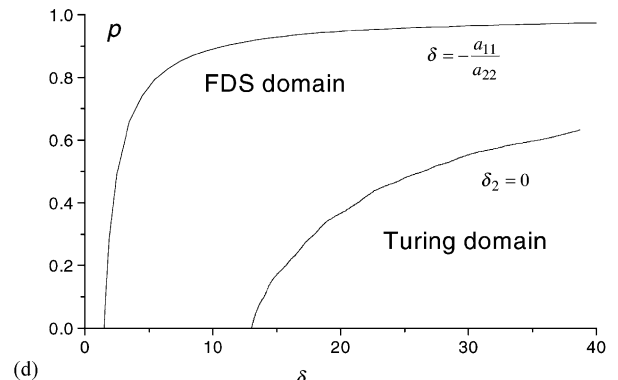
(a)



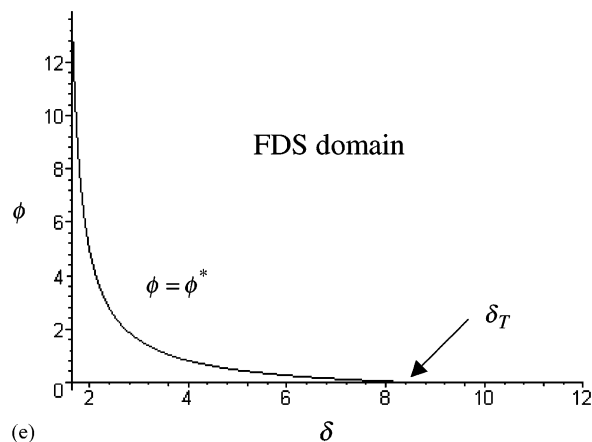
(b)



(c)



(d)



(e)

In Fig. 1a we have plotted, for the case  $\delta = 0.5$ , the boundaries of the FDS domain in the  $(\mu, p)$ -parameter plane. These are given by the two curves  $\delta_2 = \delta_2(\mu, p) = 0$  (labelled as curve 1) and  $h(\mu, \delta) = a_{11} + \delta a_{22} = 0$  (labelled as curve 3). It is instructive to discuss the location of the FDS domain in relation to the Hopf domain. For  $p = 0$  (cubic autocatalysis) the Hopf domain lies in the interval  $\mu_1 \approx 0.9003 < \mu \leq 1$  (in Fig. 1a  $\mu_1$  is labelled by  $H$ ). We see that the FDS domain does not intersect the Hopf domain. This will remain true at least in a certain vicinity around  $p \sim 0$ . We conjecture that this can be true for all of  $0 < p < 1$ . What is important from Fig. 1a is that the FDS domain is located in the region of parameter space in which the uniform steady state is locally unstable.

If we now vary  $\delta$  we see that the right hand side boundary  $h(\mu, \delta) = 0$  is shifted further to the right (for  $\delta > 1$ ) or, respectively, to the left (for  $\delta < 1$ ) from the boundary  $h(1, \mu) = \text{Tr} = 0$  corresponding to  $\delta = 1$ , which marks the case of no differential transport [11,13] and corresponds to the boundary of the Hopf domain. The FDS domain for  $\delta = 5.0$  is shown in Fig. 1b. In this case it contains a region disjoint from the Hopf region. However, this time (for example for all  $1 < \mu \leq 2.23\dots$  in the case  $p = 0$ ) the difference with Fig. 1a is that the FDS domain is located in the parameter region where  $S$  is temporally stable. Both these results are very surprising in view of the results presented in [11,13] where the existence of the flow sustained stationary waves has been claimed to require the presence of the Hopf conditions. It is also somewhat unexpected compared with [14] where the FDS domain was understood to be residing in a certain vicinity of the Hopf domain even if it could have portions outside it. We show here, for the first time, that this is not the case and in fact we can realise stationary waves for a generic reaction-diffusion model for which these waves are born out from the perturbations of the steady state when this steady state is temporally stable *only*. It cannot produce these solutions when the steady state is in the Hopf instability regime. Clearly this leads to the question of experimental verification of this prediction in view of the fact that the results in [13] do not apply.

We also note that for the two cases presented in Fig. 1a and b (i.e. when  $\delta$  is not too large) we have potential FDS instability for  $(\mu, p) \sim (0.0, 0.0)$ , i.e. for almost cubic type kinetics and weak production of the  $A$  precursor. This is surprising and a new feature for this type of model as it is known [23,24] that for the pure kinetics system ((2.4) and (2.5)) there is no bounded attractor with the solution evolving as  $(a, b) \sim (\mu t, 0)$  as  $t \rightarrow \infty$ . Thus, the inclusion of diffusion and advection increases the domain of pattern formation considerably.

---

Fig. 1. (a) Plot of the FDS domain for the quadratic-cubic system ((2.4) and (2.5)). Here  $\delta = 0.5$  and the FDS domain (shaded) lies between curves 1 and 3. The uniform steady state loses stability on curve 2 (Hopf bifurcation).  $H$  denotes the boundary point ( $\mu_1 \approx 0.9003$ ) of the Hopf domain which, for  $p = 0$ , lies in the interval  $\mu_1 \leq \mu \leq 1$ . The Hopf curve is defined as the locus of those points for which  $\text{Tr} = a_{11} + a_{22} = 0$ .  $\delta_2$  is the larger of the two roots in Eq. (3.16). (b) Plot of the FDS domain for the quadratic-cubic system ((2.4) and (2.5)). Here  $\delta = 5.0$  and the FDS domain (shaded) lies between curves 1 and 3. Note that in neither case ((a) and (b)) do we have FDS instability for the pure quadratic case. Also in both the above examples the classical Turing instability does not occur. The labelling of the curves is as defined in (a). (c) The FDS domain for the case  $\delta = 10.0$  (shaded region lying between curves 1 and 3) for the system ((2.4) and (2.5)). Note that for  $0 \leq p \leq p_0 = 0.4\dots$  the entire FDS domain is outside and well away from the Hopf domain. Here the Turing domain exists in the bounded, “angular” region surrounded by the curves 1 and 2 and exists for values in the range  $0 \leq p \leq p_0 = 0.4\dots$ . In particular there is no Turing bifurcation for the pure quadratic case. Note also the larger extent of the FDS domain as compared to the Turing domain. The labelling of the curves is as defined in (a). (d) A plot in the  $(\delta, p)$ -plane showing the extent of the FDS and Turing regions for the system ((2.4) and (2.5)). Both the Turing and FDS boundaries converge in the limit as  $\delta \rightarrow \infty$  to  $p = 1$ . (e) A plot in the  $(\delta, \phi)$ -plane of the generalised FDS domain for the pure cubic kinetics model ((2.4) and (2.5)) with  $p = 0$ . Here it is drawn for  $\mu = 1.2$ . The Turing critical diffusion is  $\delta_T = (3 + 2\sqrt{2})\mu^2 \approx 8.39$ . The pure Turing domain resides in the region  $\phi = 0$ ,  $\delta \geq \delta_T$  along the  $\delta$ -axes whereas the FDS domain lies in the whole domain bounded below by the curve  $\phi = \phi^*$  from Eq. (3.13). Note the balance in the spatial transport needed to achieve spatial patterns:  $\phi^* \rightarrow \infty$  as  $\delta$  becomes small and  $\phi^* \rightarrow 0$  as  $\delta \rightarrow \infty$  giving hyperbolae-shape behaviour.

A key issue is to compare the extent of the FDS and the Turing domains (and implicitly the locations of their boundaries) when the two kinetics parameters ( $\mu, p$ ) vary in the region where the steady state ( $a_s, b_s$ ) is temporally stable. This is shown in Fig. 1c for the case  $\delta = 10.0$ . We see that the domains for FDS and for Turing instabilities are separated by the boundary  $\delta_2(\mu, p) = 0$  (see [26] for details on Turing instabilities for the pure cubic model). Clearly the former is considerably larger than the latter. This is further substantiated in Fig. 1d, which displays the boundaries of the FDS and Turing domains in the  $(\delta, p)$ -plane for a fixed value of the kinetics parameter  $\mu$ . Clearly the size of the FDS region is greater than the corresponding Turing region. The calculations also show that both curves approach  $p = 1$  as  $\delta \rightarrow \infty$  monotonically. However, note the rapid increase in the FDS boundary up to  $\delta \approx 8.5$  followed by a slow, almost flat approach to  $p = 1$ . In contrast, the Turing curve starts off only at  $\delta \approx 13.5$  and remains always below the FDS boundary. This behaviour occurred in all the calculations we performed leading us to conjecture that it is a generic feature.

Also from Fig. 1a–d we can make a qualitative comparison between the influence of the nonlinearity for these two spatial instability mechanisms. Fig. 1d shows that increasing the differential transport between the two key species (i.e. increasing  $\delta$ ) leads to an increase in the likelihood of pattern formation in both the FDS and the Turing cases.

The features seen in these graphs can be readily understood from the general theory of the previous section. For the present kinetic scheme, relation (3.12) gives the critical wave number for FDS instability as

$$|k_c^2| = \mu \left( \frac{p^2 - 2\mu p^2 + 2\mu p + \mu^2 - 2\mu^2 p + \mu^2 p^2 - \delta(1-p)}{2\delta(\mu p - p - \mu)} \right) \quad (3.27)$$

This can exist only when  $a_{11} + \delta a_{22} > 0$  and approaches  $\mu/(2\delta)$  as  $p \rightarrow 1^-$ . The latter condition leads to a quadratic in  $p$  with the condition that the FDS instability exists only for values of  $p$  lying between the two roots of this quadratic. As one root is negative we obtain the condition

$$0 \leq p < \frac{(2\mu^2 - 2\mu - \delta) + \sqrt{(2\mu^2 - 2\mu - \delta)^2 + 4(\delta - \mu^2)(\mu - 1)^2}}{2(\mu - 1)^2} \quad (3.28)$$

for the domain of the kinetic parameters ( $\mu, p$ ) for which the instability exists. We see, for example, that there is no FDS instability for the pure quadratic case ( $p = 1$ ) since, from Eq. (3.28), this would require

$$2(\mu - 1)^2 < (2\mu^2 - 2\mu - \delta) + \sqrt{(2\mu^2 - 2\mu - \delta)^2 + 4(\delta - \mu^2)(\mu - 1)^2}$$

implying that  $1 < 0$ . However, for any  $\varepsilon > 0$  with  $0 \leq p = 1 - \varepsilon < 1$ , FDS can be realised if  $\delta \geq \delta_{\varepsilon, \mu}^* = ((1 + (\mu - 1)\varepsilon)^2)/\varepsilon$ . This shows that  $\delta_{\varepsilon, \mu}^* \rightarrow \infty$  as  $\varepsilon \rightarrow 0$ . From Eq. (3.13) we then have that the critical FDS value has  $\phi^* \rightarrow \infty$  as  $O(\delta_{\varepsilon, \mu}^*)$ . The same conclusion is valid for the Turing case. Indeed relation Eq. (3.16), which defines the Turing boundary, implies that the critical diffusion ratio  $\delta_T$  for Turing patterns satisfies

$$\delta_T = \frac{2\Delta - a_{11}a_{22} + 2\sqrt{\Delta^2 - \Delta a_{11}a_{22}}}{a_{22}^2} \quad (3.29)$$

but

$$a_{22} = \mu \left( \frac{1-p}{p + \mu - \mu p} \right) \rightarrow 0 \quad \text{as } p \rightarrow 1 \quad \text{so } \delta_T \rightarrow \infty \quad \text{as } p \rightarrow 1^- \quad (3.30)$$

Thus, we have shown that neither FDS nor Turing instabilities can exist for the pure limiting case of quadratic autocatalysis (this is consistent with the plots in Fig. 1c and d for system (2.4) and (2.5)). This type of nonlinearity isolates itself as a singular case (which is also consistent with previous studies on this type of autocatalysis in other

contexts [19]). However, there is still one marked difference here. From Fig. 1c and d and also more generally for all the other cases tried, we have found that the FDS domain asymptotically approaches values of  $(\mu, p)$  with  $p \rightarrow 1$  as  $\delta \rightarrow \infty$  ‘before’ the Turing domain does so. This of course requires, from Eq. (3.13), that the corresponding flow rate  $\phi^* = \phi^*(\mu, p) \rightarrow \infty$  as  $O(\delta)$ . Thus, the pure quadratic case itself is a limiting case which does not promote FDS. This strengthens our conclusion that it is much easier to sustain stationary patterns via the FDS route than the Turing scenario.

Fig. 1e summarises our main result. It displays the universal behaviour of the FDS mechanism which incorporates the Turing instability as a particular case. Note the balance in the spatial transport needed to achieve nonuniform patterns:  $\phi^* \rightarrow \infty$  as  $\delta$  becomes small and  $\phi^* \rightarrow 0$  as  $\delta \rightarrow \infty$  giving hyperbolae-shape behaviour. As we shall show in [37] the new FDS domain constitutes to date the most general spatial patterning domain that incorporates all the known available mechanisms: Turing, DIFI and FDO.

We have explored numerically the spatio-temporal behaviour of the above model, using Fig. 1c as a guide to choosing parameters. For the numerics we have used zero flux boundary conditions

$$\frac{\partial a}{\partial x} = 0, \quad \frac{\partial b}{\partial x} = 0$$

at  $x = 0, L$  (where 0 is the position of the inflow boundary and  $L > 0$  gives the location of the outflow boundary). Typical results are shown in Fig. 2a–c. Fig. 2a is a plot of the profiles of the solutions for system ((2.4) and (2.5)) for a point in the FDS-Hopf region (Fig. 1c). Note that the solutions are neither in phase nor out of phase, but that the phase shift lies between 0 and  $\pi$  [40]. This is the hallmark of reaction-diffusion-advection systems as compared to reaction-diffusion systems. Fig. 2b illustrates the solutions for a point in the Turing region in Fig. 1c. Here the solutions oscillate in opposite phase—a typical feature of a Turing solution for this type of kinetics. Finally, Fig. 2c shows a plot of the solutions for a point in the full FDS region in Fig. 1c. Note the flow driven resonance phenomenon in the solutions leading to greatly enhanced amplitude in the autocatalyst concentration. We have also explored FDS solutions for pure quadratic autocatalysis numerically but found that the boundary perturbation imposed in the system is washed out leading to decay to the steady, uniform state in accord with the theory above.

It is worth commenting here upon a particular feature of the FDS solutions. As it was defined the instability mechanism relies on the constant boundary source signal (Dirichlet boundary condition). We wanted to see if similar behaviour could be obtained if one changes the location of the signal from the boundary to some internal point(s) in the domain. A few numerical simulations (where the same system (2.4) and (2.5)) was solved but with condition (2.6) replaced by zero flux at  $x = 0$  instead) have shown that indeed the behaviour is similar to the original, as expected. Our considerations in Section 5 explain that this is linked with the convective nature of the FDS instability. This may have important implications for biological modelling. For example many biological morphogenetic processes proceed in a sequential order (e.g. limb and organ development in animals or plant development) and thus require the spatial instability of the model to have a convective character. As Turing instability is absolute [15] these phenomena cannot be easily modelled in a standard reaction-diffusion context.

We have also attempted a test for the sensitivity to parameter variation of the FDS and Turing mechanisms. There are many ways in which this could be done. A difficulty here is to find a test which allows for a consistent comparison of the spatial mechanisms. One simple one is illustrated in Fig. 2d. From the patterning domains given in Fig. 1c we can fix a set of parameter values (well inside each domain for each case). One then asks what are the changes in solution characteristics when the parameters are varied in some range, say within  $\pm 20\%$  from their initial values. This was implemented by studying in detail the variation in pattern wavelengths computed from the numerical solutions. Fig. 2d illustrates the result for a typical case. The y-axis displays the average percentage change in the wavelength as a function of the percentage change in parameter. This measure resembles a linear correlation coefficient between the two quantities. One sees that both mechanisms are relatively robust to the changes

in parameters with all the cases showing that the solutions are less than proportional to changes in the input values. For both FDS and Turing solutions the response to changes in  $p$  is very small; variations in  $\mu$  give a response of about 50% change; variations in the diffusion ratio  $\delta$  lead to a change of about 30%. We draw attention to the fact that the sensitivity of the patterns in the Turing case is always greater than for the FDS solution for comparable parameters ( $\phi = 0$ ). This is best illustrated in Fig. 2e. This displays the concentration profile in the autocatalyst species for the two cases of FDS and Turing, respectively, when all the parameters are fixed except  $p$  (which is related to the linear interpolation in the kinetics steps). We clearly see the high sensitivity in the amplitude of the

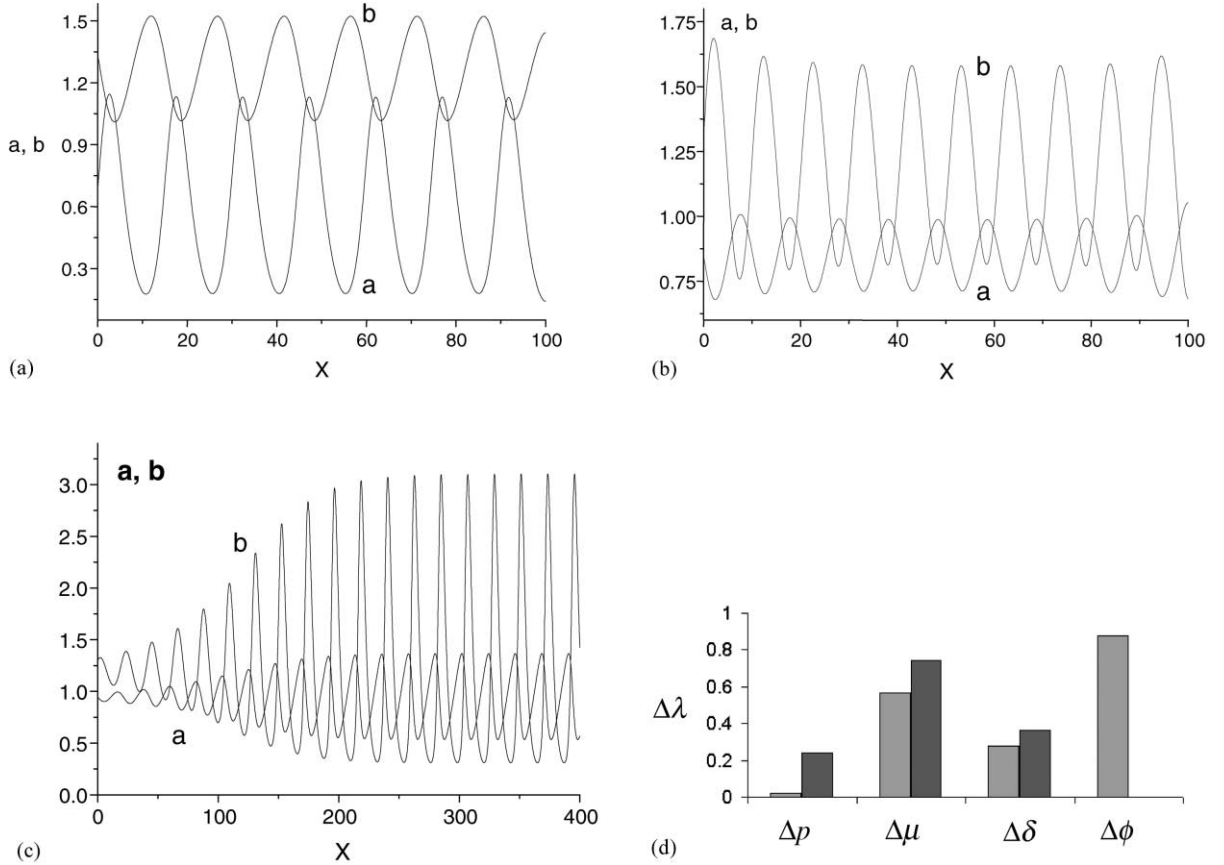


Fig. 2. (a) Plot of the solutions for the case  $\delta = 10.0$ ,  $\mu = 0.58$ ,  $p = 0.4$ ,  $\phi = 0.3$  for the system ((2.4) and (2.5)). Here  $\phi_c \approx 0.28$  and we are in the FDS-Hopf region in Fig. 1c. In Fig. 1(a)–(c) the solution was plotted after a sufficiently long time had elapsed to allow the structure to reach a steady form. (b) Plot of the solutions for the case  $\delta = 10.0$ ,  $\mu = 1.2$ ,  $p = 0.1$ ,  $\phi = 0.1$  for the system ((2.4) and (2.5)). Here  $\phi_c = 0$  and we are in the Turing region in Fig. 1c. Note that the solutions oscillate in opposite phase, as is typical for a Turing type solution for this type of kinetics. (c) A plot of the solutions for the system ((2.4) and (2.5)) in the case  $\delta = 10.0$ ,  $\mu = 1.2$ ,  $p = 0.7$ ,  $\phi = 1.2$ . Here  $\phi_c = 1.044$  and we are in the full FDS region in Fig. 1c. Note the resonant phenomenon in the solutions driven by the flow leading to enhanced amplitude in the concentration of the autocatalyst,  $b$ . (d) Results of the sensitivity analysis of the FDS and Turing patterns to parameter variations. This figure displays the percentage change in solution wavelength as function of  $\pm 20\%$  change in parameter values. The lighter shading corresponds to FDS and darker shading to the Turing cases, respectively. Note that FDS solutions (i.e.  $\phi > 0$ ) are more robust than the Turing solutions. (e) A comparison of the solution sensitivity to variation in the parameter changes for system ((2.4) and (2.5)) for FDS and Turing cases, respectively. The parameter values are  $\delta = 11.0$ ,  $\mu = 1.2$ ,  $\phi = 1.1$ . For each case  $\pm 20\%$  variation in the linear interpolation parameter  $p$  was computed from the chosen value  $p = 0.1$ . Note the high sensitivity in the amplitude of the solutions in the Turing case as compared to the FDS case. The same remark applies to the variation in the wavelength.

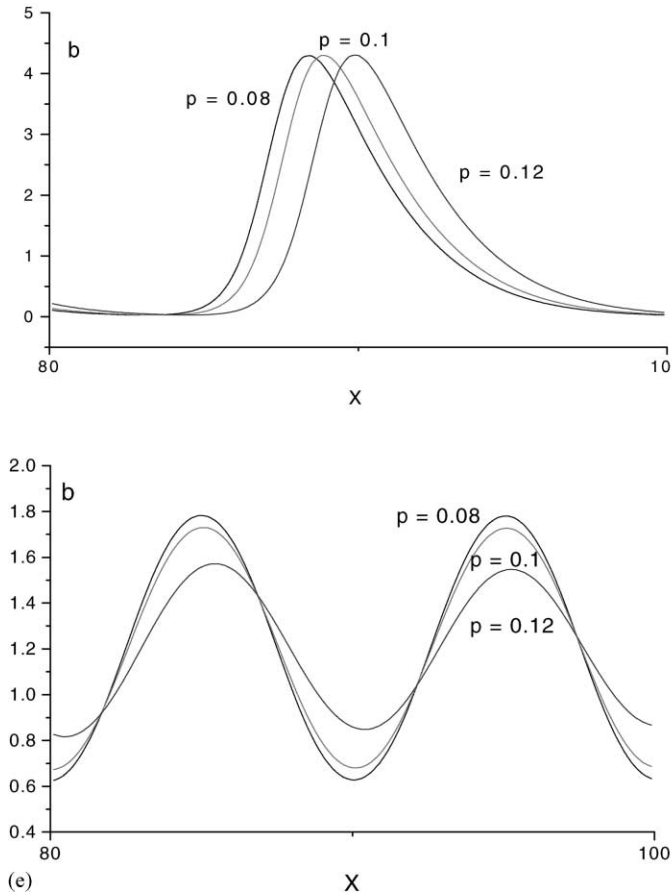


Fig. 2. (Continued).

solution for the Turing case as compared to the FDS case illustrating the robustness of the patterning mechanism in the presence of both flow and diffusion. However, there is a relatively large change in the mean wavelength as the advection rate is varied. The reason for this is our previous findings [14] that the selected wavelength pattern scales proportionally with the flow rate (hence the values close to 1, or linear dependence in the sensitivity analysis).

To summarise, the above the parameter constraints for FDS instability giving rise to stationary, spatially varying patterns for the case of  $S$  being initially temporally stable are much less stringent than those for Turing instability [7]. Specifically, the requirement on the diffusion ratio  $\delta$  is less restricted thus making FDS easier to be physically realised [13,14]. The requirements on the nonlinearity are also more flexible and the kinetics parameter domain is considerably extended. Our pattern sensitivity studies illustrated in Fig. 2d show that the FDS mechanism is more robust to variations in parameters despite using one more parameter and having enhanced spatial dynamics requirements (i.e. variations in both diffusion and flow). All these properties make the FDS instability a robust phenomenon. The numerical simulations strongly suggest that the FDS parameter domain is of considerably greater extent than the Turing domain. On the basis of the above generic model, given the more enhanced likelihood for the FDS waves to occur in pattern formation than the corresponding Turing waves, we conclude that the FDS mechanism is a more robust pattern generator than the Turing mechanism.

### 3.2.2. Quadratic–cubic power interpolation model

We now consider a different type of nonlinearity still based on the generic steps in Eqs. (2.4) and (2.5). Specifically we replace the two steps in reactions (2.2.1) and (2.2.2) by



where  $1 \leq m$ . For  $m = 1$  we have the step (2.2.1) (pure quadratic autocatalysis) while  $m = 2$  is step (2.2.2) (pure cubic autocatalysis). Therefore, we have  $f(a, b) = \mu - ab^m$ ,  $g = ab^m - b$ . The results are presented in Fig. 3a–c. We see from all these figures that for  $m \rightarrow 1$  (quadratic autocatalysis) the FDS domain becomes singular and shrinks to the point  $(m, \mu) = (1, 0)$ . In this case the required critical flow rate is infinite as can be computed directly from Eq. (3.13) for these parameter values. For any given  $\delta > 0$ ,  $m > 1$  we have a finite range of values for the parameter  $\mu$  such that FDS exists for values in that range and flow rates above the corresponding critical flow rate from Eq. (3.13).

It is again instructive to compare the Turing and FDS domain sizes. In Fig. 3c we plot the Turing domain boundary  $\delta_2 = \delta_2(\mu, m) = 0$  (curve 1), the Hopf domain boundary (curve 2) and the right-hand side boundary of the FDS

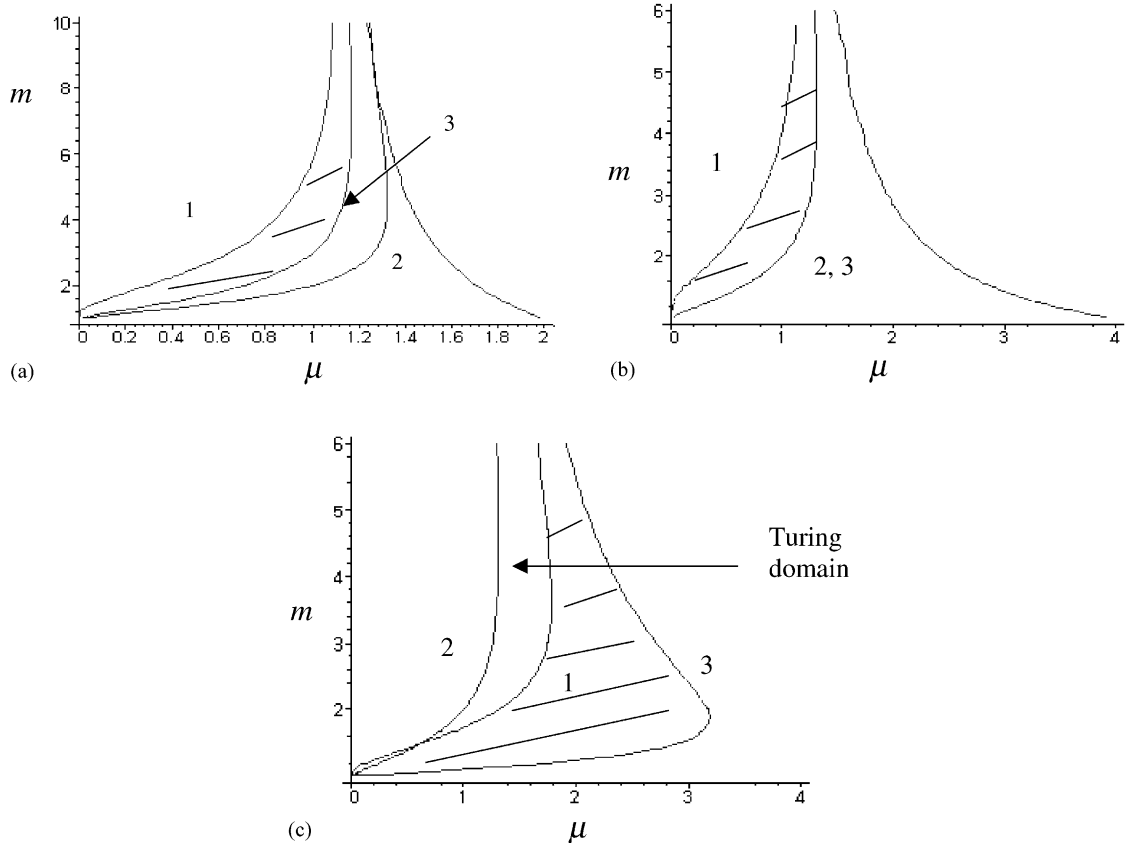


Fig. 3. (a) Plot of the FDS domain (shaded region between curves 1 and 3) for  $\delta = 0.5$  for the power interpolation model ((3.5) and (3.6)). The labelling of the curves is as defined in Fig. 1a. (b) Plot of the FDS domain (shaded region between curves 1 and 2 (or 3—for this case curves 2 and 3 coincide)) for  $\delta = 1.0$  for the power interpolation model described in Section 3.2.2. The labelling of the curves is as defined in Fig. 1a. (c) Plot of the FDS domain (shaded region between curves 1 and 3) for  $\delta = 10.0$  for the power interpolation model described in Section 3.2.2. The Turing domain lies between curves 1 and 2 for  $m > 1.21$ . The labelling of the curves is as defined in Fig. 1a.

domain  $a_{11} + \delta a_{22} = (m - 1)\delta - \mu^m = 0$  (curve 3). For  $m \rightarrow \infty$  the  $\mu$ -range of both Turing and FDS domains shrink to a point. Indeed, for given  $\delta > 0$ ,  $m > 1$  the Hopf boundary is located at  $\mu_1 = \sqrt[m]{m-1}$  whereas the FDS domain boundary corresponds to  $\mu_2 = \sqrt[m]{d(m-1)}$ . It is, therefore, clear that  $\mu_2 \rightarrow \mu_1$  as  $m \rightarrow \infty$  for fixed  $\delta > 0$ . From Fig. 3c it is also clear that the extent of the FDS domain is much greater than the corresponding size of the Turing domain hence the results are similar to those from the previous application. We found this to be true for all values of  $\delta > 1$  tried.

### 3.2.3. Comparison with other classical kinetic models

Following the general results above we have explored the FDS and Turing patterning domains for a variety of nonlinear kinetics schemes that are used widely in chemistry and biology. These include the following systems: Gierer–Meinhardt, Schnakenberg, CIMA and Thomas kinetics [7,8,28,29,33,36]. Our two previous schemes have served as generic templates for comparison between domains. The CIMA system (chlorite-iodide-malonic acid-starch reaction) is relevant since it was used for the first experimental realisation of Turing structures [5,6]. A two variable model for the CIMA reaction is presented in [29]. Starch immobilises molecular iodine by forming an inclusion compound. This increases the ratio of diffusion coefficients and moves the parameters into the regime of Turing instability. The dimensionless governing equations are:

$$\frac{\partial a}{\partial t} = \delta \frac{\partial^2 a}{\partial x^2} - \delta \phi \frac{\partial a}{\partial x} + b - \beta \frac{ab}{1+b^2} \quad (3.32)$$

$$\frac{\partial b}{\partial t} = \frac{\partial^2 b}{\partial x^2} - \phi \frac{\partial b}{\partial x} + \alpha - b - 4\beta \frac{ab}{1+b^2} \quad (3.33)$$

Here,  $a$  is the dimensionless concentration of  $\text{ClO}_2^-$  (chlorite ion, which is an inhibitor) and  $b$  is the dimensionless concentration of  $\text{I}^-$  (iodide ion). This models a special type of self-inhibitory kinetics similar, for example, to the Thomas kinetics [7,8] employed in biochemical modelling. The nonlinearity is inhibitory in both equations whereas all previous examples employed the so-called *cooperative activation* type nonlinearity.

Eqs. (3.32) and (3.33) admit the uniform steady state

$$S = \left\{ a_s = \frac{\alpha}{5}, b_s = \frac{1 + (\alpha/5)^2}{\beta} \right\}$$

and we can apply the general results above to determine parameter domains for spatial instability. Such a result is shown in Fig. 4 for  $\delta = 15.0$ , a value typical for the experiments. The FDS instability is predicted for both the cases when  $S$  is temporally stable and unstable (Hopf domain), respectively. There is an “angular” shaped region on the right-hand side of this figure (between curves 2 and 3) where  $S$  is stable and Turing patterns are predicted. It is clear that the FDS domain is much larger in size than the corresponding Turing region. As the two key parameters  $\alpha$  and  $\beta$  are increased from zero we see that the FDS region is predicted to occur well before the Turing instability. Again it is also possible to have FDS instability even when Turing instability does not exist (for cases when FDS is entirely included in the Hopf domain or when it intersects it).

The linear stability calculations backed by simulations reveal that the qualitative picture of the spatial instability domains is similar for all these models. In all the cases the domain in parameter space for FDS instability is much larger than the corresponding domain for the Turing instability. Starting from a parameter set which does not allow patterning, as  $\delta$  is increased through 1 to larger values, we found that instability always occurs first via the FDS route. However, between them, the CIMA and Thomas schemes allow the largest parameter domains in comparison to Gierer–Meinhardt or Schnakenberg schemes. We also note that between the two generic schemes studied in Sections 3.2.1 and 3.2.2 the power interpolation model generates smaller patterning domains than the linear interpolation counterpart. Finally, preliminary studies reveal that FDS waves exist for both bistable and

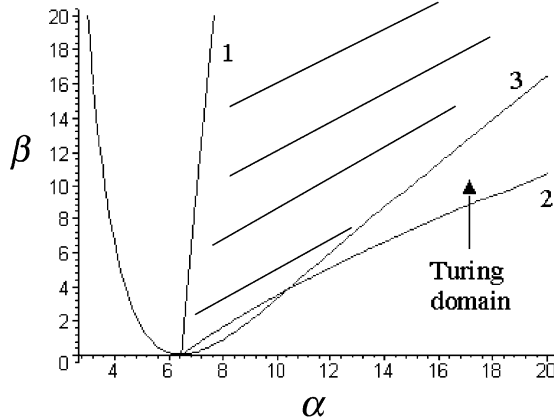


Fig. 4. A typical plot of the spatial instability domains for the CIMA kinetics described in Section 3.2.4. The FDS domain (shaded) is surrounded by the curves 1 and 3. Curve 2 is as defined in Fig. 1. The Turing domain lies between curves 2 and 3 for  $\beta \geq 3.8$ . The labelling of the curves is as defined in Fig. 1a.

excitable kinetics (for example, FitzHugh–Nagumo FHN [40,41] and Belousov–Zhabotinskii BZ [42,43] kinetics). A more detailed analysis of these cases will be presented elsewhere [38].

#### 4. Nonlinear analysis of the FDS solutions

We now look at the FDS solutions in more detail. The previous linear analysis determined the regions in parameter space where the FDS solutions are expected. However, in order to gain insight into the form of these periodic solutions we need to consider the full nonlinear system. Our goal is to understand the variations in the solution characteristics (wavelength, amplitude) with the parameters. The method we use can be applied to any bifurcation to stationary solutions and therefore is applicable for analysing both FDS and Turing patterns. The idea is to regard the bifurcation to stationary space periodic solutions in the PDE case as corresponding to a Hopf bifurcation to periodic solutions for the reduced elliptic, ODE system. For the latter we can use a standard continuation method which follows nontrivial branches of bifurcating solutions (stationary, spatial periodic) from the Hopf point corresponding to the FDS bifurcation. This is complemented by a shooting method to integrate the nonlinear system as described below. This method reduces the analysis of the full PDE system to that of the associated elliptic ODE part which is considerably easier. Furthermore, it has the advantage of giving quantitative insight into the solution structure in a wider parameter space than that which is accessible through an envelope equation formalism. By way of illustration, we carry out the analysis for the main model used here ((2.4) and (2.5)). We shall do this for the case  $p = 1$  (cubic case) but there is no difficulty in extending this to other values of  $p$ ,  $0 < p < 1$ .

Suppose that the system ((2.4) and (2.5)) has stationary solutions of the form  $a = a(x)$ ,  $b = b(x)$ . Then

$$\delta a'' - \delta \phi a' + \mu - ab^2 = 0 \quad (4.1)$$

$$b'' - \phi b' + ab^2 - b = 0 \quad (4.2)$$

where prime denotes differentiation with respect to  $x$ . Since we are looking for stable periodic solutions to Eqs. (4.1) and (4.2) we solve the above system subject to periodic boundary conditions

$$a(0) = a(\lambda), \quad b(0) = b(\lambda), \quad a'(0) = a'(\lambda), \quad b'(0) = b'(\lambda) \quad (4.3)$$

(since we are looking for periodic solutions there is no loss in generality in taking the left boundary condition to be at  $x = 0$ ). In Eq. (4.3)  $\lambda$  is the wavelength of the solution (clearly any solution to Eqs. (4.1) and (4.2) corresponds to a solution to the initial system ((2.4) and 2.5))). Problem ((4.1)–(4.3)) is a nonlinear boundary-value problem (bvp) in  $a$ ,  $b$  and  $\lambda$ . We begin the analysis with a general property of the solutions.

**P1.** Every solution pair  $(a, b)$  to the bvp (4.1)–(4.3) has  $a > 0$ ,  $b > 0$ .

**Proof.** For the full system ((2.4) and (2.5)) it can be shown in general (via invariant region methods) that every solution beginning with positive initial conditions remains positive for all times. Thus, we only need to show that there is no solution to system (4.1)–(4.3) passing through zero. Suppose that there is a point  $x_0$ ,  $0 \leq x_0 \leq \lambda$ , with  $a(x_0) = 0$ . Then we require  $a'(x_0) = 0$ ,  $a''(x_0) \geq 0$  for the solution to remain non-negative. Clearly we then have a contradiction from Eq. (4.1) since  $0 = \delta a''(x_0) + \mu > 0$ . Suppose now that there is an  $x_1$  such that  $b(x_1) = 0$ . As above we deduce that  $b'(x_1) = 0$ ,  $b''(x_1) \geq 0$ . From Eq. (4.2) we then have that  $b''(x_1) = 0$ . Clearly we can repeat the above argument to any higher order derivative in  $b$  and deduce that  $b^{(n)}(x_1) = 0$  for all positive integers  $n$ . This leads to the unique trivial solution  $b \equiv 0$  via the uniqueness property of the solutions which is a contradiction and establishes the result.  $\square$

Periodic solutions to system (4.1)–(4.3) bifurcate from the steady state through a Hopf bifurcation. This leads us to study the stability of the steady state  $S = \{(1/\mu), \mu\}$  of (4.1)–(4.3) in terms of the spatial co-ordinate  $x$ . Consider small perturbations to  $S$  of the form

$$a = \frac{1}{\mu} + A, \quad b = \mu + B \quad (4.4)$$

where  $0 < |A| \ll a$ ,  $0 < |B| \ll b$ . The resulting linear system in  $(A, B)$  is solved by looking for solutions proportional to  $e^{\gamma x}$ . We find that the eigenvalue  $\gamma$  must satisfy the quartic

$$\delta\gamma^4 - 2\delta\gamma^3\phi + (\delta + \delta\phi^2 - \mu^2)\gamma^2 + \phi\gamma(\mu^2 - \delta) + \mu^2 = 0 \quad (4.5)$$

At the Hopf bifurcation we require that  $\gamma$  is purely imaginary,  $\gamma = i\eta$ ,  $\eta = (2\pi/\lambda) > 0$ . This leads to the two conditions

$$\delta\eta^4 + \eta^2(\mu^2 - \delta - \delta\phi^2) + \mu^2 = 0, \quad 2\delta\eta^2 = \delta - \mu^2 \quad (4.6)$$

From Eq. (4.6) we obtain the neutral curve (the value of  $\phi$  at the bifurcation point)

$$\phi_c^2 = \phi^2(\mu, \delta) = -\frac{1}{2} \frac{\delta^2 - 6\delta\mu^2 + \mu^4}{\delta(\delta - \mu^2)} \quad (4.7)$$

The neutral curve (4.7) is the same as the one obtained from the linear theory in Section 3, as expected. We deduce that stationary periodic solutions appear only when the right hand side of Eq. (4.7) is positive and we expect that  $\phi \geq \phi_c(\mu, \delta)$ . This is confirmed by the numerical results below. Furthermore, from Eq. (4.6) we find also the value of the Hopf frequency  $\eta$  as

$$\eta = \sqrt{\frac{\delta - \mu^2}{2\delta}} \quad (4.8)$$

and therefore the wavelength of the periodic solution at bifurcation is

$$\lambda = 2\pi \sqrt{\frac{2\delta}{\delta - \mu^2}} \quad (4.9)$$

These results agree with our previous calculations in [14].

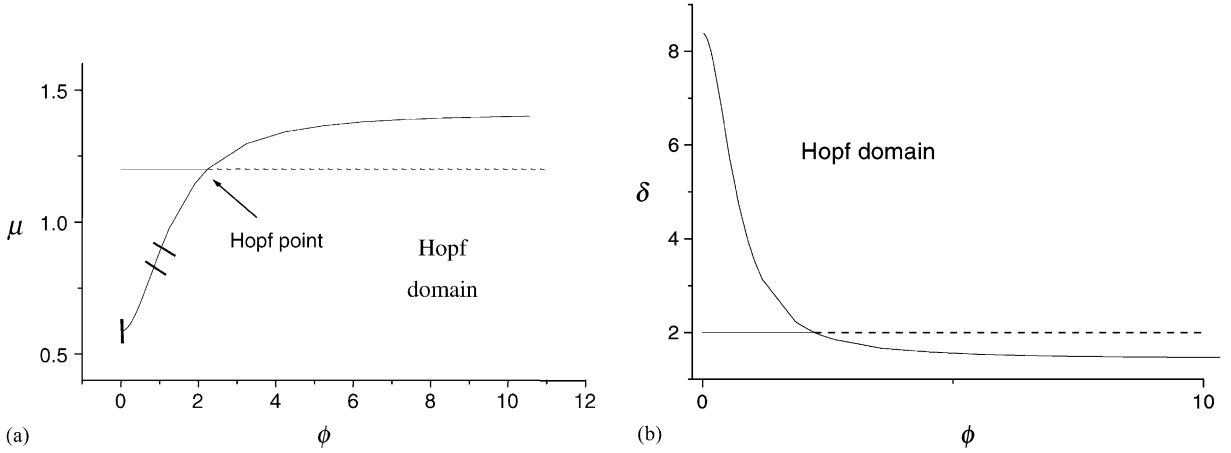


Fig. 5. (a) Bifurcation diagram showing the region of periodic solutions in the  $(\phi, \mu)$ -plane for system ((4.1)–(4.3)). The continuous straight line corresponds to the continuation of the uniform steady state at  $\mu = 1.2, \delta = 2.0$ . The Hopf bifurcation point is located at  $\mu = 1.2, \phi = 2.2503$  and is a supercritical bifurcation. The Hopf curve was followed in the range  $0.02 < \phi < 11.0$  although it exists in reality for any  $\phi > 0$ . Between the two points, (1.056, 0.909) and (1.908, 1.145) (marked with segments on the Hopf curve), the periodic solutions are unstable. The dotted line signifies that the steady state is unstable inside the Hopf region. (b) Bifurcation diagram in the  $(\phi, \delta)$ -plane for the uniform steady state in the case  $\mu = 1.2$  for system ((4.1)–(4.3)). The Hopf domain is defined for  $1 < \delta_c \leq \delta \leq 8.35$ . The dashed line denotes the unstable steady state inside the Hopf domain.

To continue the bifurcating solutions beyond the Hopf point we have to resort to numerical techniques. We determine the bifurcating branch by using the bifurcation package LOCBIF [30]. This has the advantage of providing further details about the nature/stability of the solution. A typical bifurcation diagram is shown in Fig. 5a in the  $(\phi, \mu)$ -plane and reveals that there is a minimum value of  $\mu$ ,  $\mu_{\min}$ , such that periodic solutions exist for  $\mu \geq \mu_{\min}$  for all  $\phi > 0$ . Although the Hopf curve is defined for all  $\phi > 0$  the results in Fig. 5a suggest that there is also a maximum value of  $\mu$ ,  $\mu_{\max}$ , with periodic solutions (stationary waves) existing only for  $\mu \leq \mu_{\max}$ . These observations agree with our analytical results in Section 3. The calculations also show that the Hopf bifurcation is supercritical generically with only a relatively small range  $0.909 < \mu < 1.145$  where the bifurcation is subcritical (denoted by two small segments on the Hopf curve in Fig. 5a). Fig. 5b displays the behaviour in the  $(\phi, \delta)$ -plane for  $\mu = 1.2$ . Oscillatory solutions (FDS waves) exist for all  $\phi > 0$  and  $1 < \delta_c \leq \delta \leq 8.35$ . When checked analytically these values agree with the results derived in Section 3.

The periodic solutions along the Hopf branch have been computed by solving Eqs. (4.1)–(4.3) using a standard shooting method as implemented by the NAG library routine DO2AGF. The results are illustrated in Fig. 6 for two representative cases. In Fig. 6a we show a graph of the amplitude of the stationary, space periodic solutions for  $b$  for a range of values of flow rates, starting from the Hopf point and increasing the flow rate inside the oscillatory domain. This curve has the characteristic form of a Hopf bifurcation curve. Fig. 6b shows profiles of  $b$  for four flow rates chosen from the values used in Fig. 6a. We can see clearly the change in the solution profile from a harmonic type wave (for  $\phi = 1.84$  close to the Hopf point in this case) towards a wave type with a rapid “burst spike” followed by a longer decay tail reminiscent in form of waves seen in excitable media. Finally in Fig. 6c we show the solutions for a case when the uniform steady state of the system ((2.4) and (2.5)) with  $p = 1$  is temporally stable. This figure clearly shows that when  $a$  decays  $b$  grows and vice versa even if here the solution profiles differ in phase by a quantity which is not an integer multiple of  $\pi$ . Our results confirm the linear dependence of the wavelength with the flow rate for the cases tried.

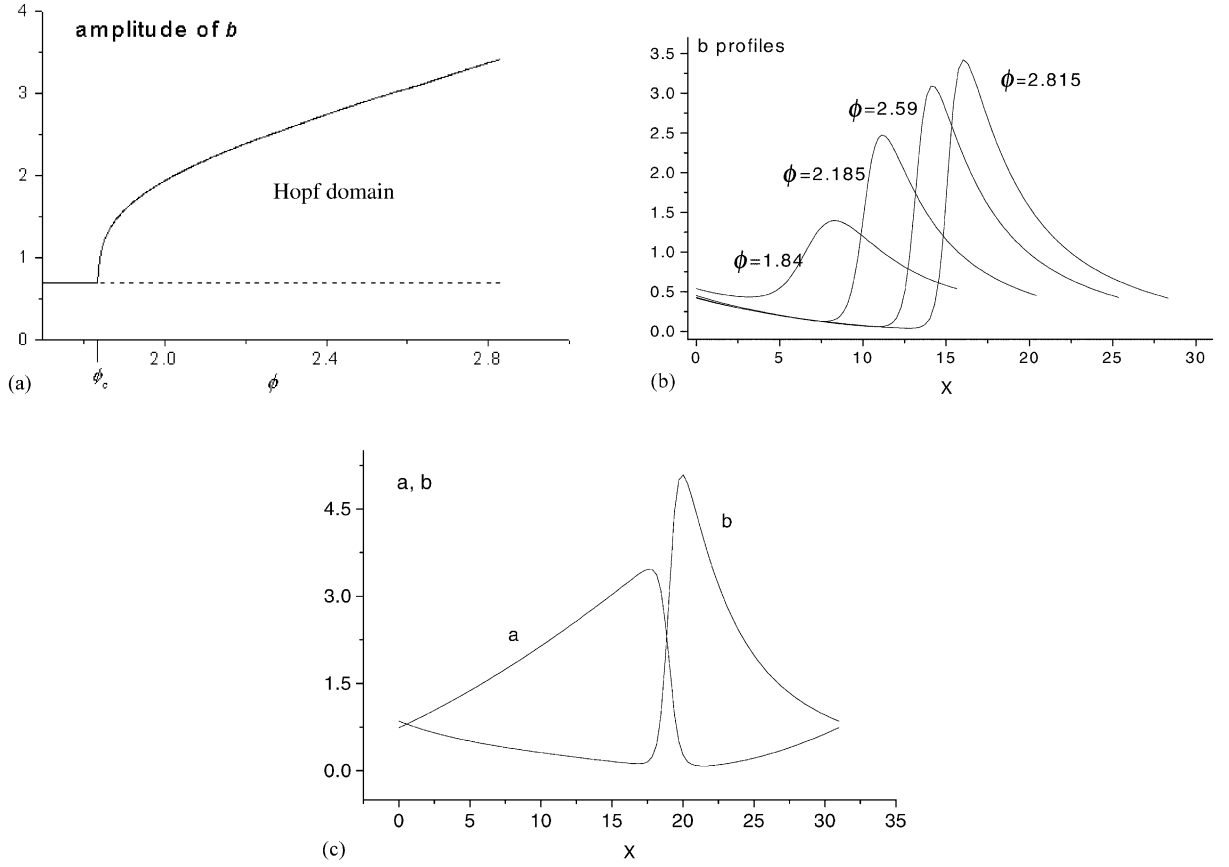


Fig. 6. (a) Bifurcation diagram for system ((4.1)–(4.3)): plot of the amplitude of the periodic solution profile of  $b$  as a function of the electric field intensity for a range of values of  $\phi$  starting from the Hopf bifurcation value  $\phi \approx 1.837$ . Here,  $\delta = 1.0$ ,  $\mu = 0.8$ . The continuous line corresponds to the stable solutions. The dashed line represents the unstable steady state inside the Hopf domain. (b) A plot of the stationary waves in the autocatalyst concentration  $b$  for  $\delta = 1.0$ ,  $\mu = 0.8$  and different values of the electric field  $\phi$  for system ((4.1)–(4.3)). (c) The stationary solutions for the system ((4.1)–(4.3)) found with the NAG library routine DO2AGF for the case  $\delta = 2.0$ ,  $\mu = 1.2$ ,  $\phi = 30$ . Here  $\lambda = 30.98$ .

## 5. Conclusions and discussion

Our analysis has highlighted key features of the new FDS spatial instability mechanism. For the models studied here, which all employ generic kinetics steps, and for the case when the uniform steady state is temporally stable (which is the more relevant case in applications to morphogenesis) the parameter regime in which the FDS instability occurs is much larger than that for the Turing instability. In particular, we have shown that the restrictions on the differential diffusion rate required for Turing is considerably relaxed for FDS. The most striking result of the analysis is the greater ease, compared to pure diffusion, with which the combined action of advection and diffusion induces spatial instability. In particular, FDS always sets in at lower values of the transport ratio  $\delta$  than does the Turing instability. This means that FDS is more likely to occur in biological and artificial reaction-advection-diffusion systems, particularly since FDS may be realised even when  $\delta < 1$ . The case  $\delta = 1$  (no differential transport) has been analysed before by linear stability [11,12] and by phase dynamics [27,38] and it has been realised by experiment [13,27]. On the other hand, when  $S$  is temporally unstable, the FDS and Turing domains are similar. For

comparison purposes we have extended the Turing case to this latter situation. Our analysis has clearly shown that one can naturally introduce the FDS concept across the whole range of  $0 < \delta < \infty$  (Fig. 1e). This makes it appealing in a biological modelling context where one has to deal with species with very different transport properties, be it through their different molecular weights or through selective immobilisation. Moreover the signal can be located anywhere in the spatial domain (not necessarily at the inflow boundary). This highlights the flexibility of the above mechanism in comparison with the Turing case when the uniform steady state is temporally stable. However, it should be noted that varying the form of the boundary conditions can enhance the parameter domain in which Turing instabilities occur [31,36]. A similar study remains to be done for the FDS.

This analysis has obvious application to chemistry. Following their theoretical prediction, the rapid experimental realisation of FDO waves in an open flow reactor [13] raises hopes that FDS can also be readily observed. In contrast the severe parameter restrictions in the Turing case were the main obstacle that delayed its experimental realisation by several decades. It is usual that reactions occur with the key species having comparable diffusion rates thus making Turing structures difficult to obtain. Our new differential transport mechanism does not suffer this restriction.

To compare FDS and Turing we have specifically considered quadratic and cubic nonlinearities, our motivation being the results in [32,33] which show that the form of the nonlinearity can greatly affect the type of pattern exhibited as a result of a Turing bifurcation. The latter focussed on pattern selection on two-dimensional domains but our analysis here was for a one-dimensional domain. We are presently carrying out a nonlinear bifurcation analysis of the FDS instability to see if similar conclusions on the effect of nonlinearity can be drawn. The study in the present paper enables us to analyse the diversity of reaction kinetics ranging from purely quadratic to purely cubic. For the purely quadratic case both FDS and Turing instabilities are impossible.

Although both FDS and Turing patterns are stationary the character of the spatial instability is different in these two cases at least when the uniform steady state is stable. While any Turing pattern (from the discussion after Eq. (3.26), this requires  $\delta \geq \delta_2$ ) is the result of an absolute instability it is possible to show that FDS occurs via a convective instability for  $1 < \delta \leq \delta_2$ . Full details will be presented elsewhere [36]. This is to be compared with the DIFI bifurcation, which can arise either as a convective or an absolute instability [17].

Our study also shows that the spatial structures formed by FDS are richer than those formed from the Turing instability, including, for example, phase differences between the maximum in the amplitude of the key species and modulation in their amplitudes. In contrast it is known that in the vicinity of primary bifurcation points, the chemical concentration profiles exhibited in a Turing system of two chemical species are either spatially in phase, or  $180^\circ$  out of phase. In the FDS case, other phase differences are possible. Perumpanani et al. [34] showed that this was also the case for a DIFI bifurcation. It has been hypothesised that cells may interpret chemical pre-patterns via phase differences rather than absolute concentration value and this has been used to account for segmentation patterning in insects [35]. However, the appropriate solutions obtained in [34] are extremely sensitive to parameter values. Here we have presented for the first time a viable, robust mechanism for generating stable phase differences between stationary wave solutions to reaction-diffusion equations. Organisms may use such phase shifts [35,39] to encode positional information with high spatial resolution.

Extensions of the current FDS scenario that allow for periodic boundary forcing may be important for biological applications [27,38]. This external forcing can replace the unstable internal modes of the system [38]. Periodic boundary forcing of active media is believed to play a key role in the formation of somites in chick and mouse [27,38].

## Acknowledgements

RAS acknowledges the financial support from the joint BBSRC/EPSRC Initiative in “Mathematical Modelling, Simulation and Prediction of Biological Systems”, Grant no. 43-MMI 09782 awarded to J.P. Armitage and P.K. Maini.

## References

- [1] A.M. Turing, The chemical basis of morphogenesis, *Phil. Trans. R. Soc. London B* 237 (1952) 37–72.
- [2] L.G. Harrison, *Kinetic Theory of Living Pattern*, Cambridge University Press, Cambridge, 1993, 354 pp.
- [3] B. Goodwin, How the Leopard Changed its Spots, Weidenfeld & Nicolson, London, 1994, 233 pp.
- [4] V. Castets, E. Dulos, J. Boissonade, P. De Kepper, *Phys. Rev. Lett.* 64 (1990) 2953–2956.
- [5] Q. Ouyang, H.L. Swinney, *Nature (London)* 352 (1991) 610.
- [6] R.A. Satnoianu, M. Menzinger, P.K. Maini, Turing instabilities in general systems, *J. Math. Biol.* 41 (2000) 493–512.
- [7] J.D. Murray, *Mathematical Biology*, Springer, Berlin, 1993.
- [8] J.D. Murray, Parameter space for Turing instability in reaction-diffusion mechanisms: a comparison of models, *J. Math. Biol.* 98 (1982) 143–163.
- [9] A.B. Rovinsky, M. Menzinger, Self-organization induced by the differential-flow of activator and inhibitor, *Phys. Rev. Lett.* 70 (1993) 778–781.
- [10] R.A. Satnoianu, Spatiotemporal structures in differential-flow reactors, PhD Thesis, University of Leeds, 1999.
- [11] P. Andrensen, M. Bache, E. Mosekilde, G. Dewel, P. Borckmans, Stationary space-periodic structures with equal diffusion coefficients, *Phys. Rev. E* 60 (1999) 297–301.
- [12] S. Kuznetsov, G. Dewel, E. Mosekilde, P. Borckmans, Absolute and convective instabilities in a one-dimensional Brusselator flow model, *J. Chem. Phys.* 106 (1997) 7609–7616.
- [13] M. Kaern, M. Menzinger, Experimental observation of stationary chemical waves in a flow system, *Phys. Rev. E* 60 (1999) 3471–3474.
- [14] R.A. Satnoianu, M. Menzinger, Non-Turing stationary patterns: flow-distributed stationary structures with general diffusion and flow rates, *Phys. Rev. E* 62 (2000) 113–119.
- [15] J.H. Merkin, R.A. Satnoianu, S.K. Scott, The development of spatial structure in an ionic chemical system induced by applied electric fields, *Dyn. Stabil. Syst.* 15 (2000) 209–230.
- [16] J.H. Merkin, H. Sevcikova, D. Smita, M. Marek, The effects of an electric field on an autocatalytic ionic reaction in a system with high ionic strength, *IMA J. Appl. Math.* 60 (1998) 1–31.
- [17] R.A. Satnoianu, J.H. Merkin, S.K. Scott, Spatio-temporal structures in a differential flow reactor with cubic autocatalator kinetics, *Phys. D* 124 (1998) 354–367.
- [18] R.A. Satnoianu, J.H. Merkin, S.K. Scott, Forced convective structures in a differential-flow reactor with cubic autocatalytic kinetics, *Dyn. Stabil. Syst.* 14 (1999) 275–298.
- [19] S.K. Scott, K. Showalter, Simple and complex propagating reaction-diffusion fronts, *J. Phys. Chem.* 96 (1992) 8702–8711.
- [20] A. Saul, K. Showalter, in: R.J. Field, M. Burger (Eds.), *Oscillations and Travelling Waves in Chemical Systems*, Wiley, New York, 1985 (Chapter 11).
- [21] D. Henry, *Geometric Theory of Semilinear Parabolic Equations*, Lecture Notes in Mathematics, Vol. 840, Springer, Berlin, 1981.
- [22] R.A. Satnoianu, Global existence properties for a class of reaction-diffusion equations of the autocatalytic type, submitted for publication.
- [23] J.H. Merkin, D.J. Needham, S.K. Scott, Oscillatory chemical reactions in closed vessels, *Proc. R. Soc. London A* 406 (1986) 299–323.
- [24] J.H. Merkin, D.J. Needham, S.K. Scott, On the creation, growth and extinction of oscillatory solutions for a simple pooled chemical reaction scheme, *SIAM J. Appl. Math.* 47 (1987) 1040–1060.
- [25] P.K. Maini, K.J. Painter, H.N.P. Chau, Spatial pattern formation in chemical and biological media, *J. Chem. Soc., Faraday Trans.* 93 (1997) 3601–3610.
- [26] R. Hill, J.H. Merkin, D.J. Needham, Stable pattern and standing wave formation in a simple isothermal cubic autocatalytic reaction scheme, *J. Eng. Math.* 29 (1995) 413–436.
- [27] M. Kaern, M. Menzinger, A. Hundig, Segmentation and somitogenesis derived from phase dynamics in growing oscillatory media, *J. Theor. Biol.* 207 (2000) 473–493.
- [28] H. Meinhardt, *Models of Biological Pattern Formation*, Academic Press, New York, 1982, 230 pp.
- [29] I. Lengyel, I. Epstein, Modelling of Turing structures in the chlorite-iodide-malonic acid-starch reaction system, *Science* 251 (1991) 650–652.
- [30] A.I. Khibnik, Y.A. Kuznetsov, V.V. Levitin, E.V. Nicolaev, LOCBIF, Version 2, CAN Expertise Centre, 1992, The Netherlands.
- [31] P.K. Maini, M.R. Myerscough, Boundary-driven instability, *Appl. Math. Lett.* 10 (1997) 1–4.
- [32] B. Ermentrout, Stripes or spots? Nonlinear effects in bifurcation of reaction-diffusion equations on the square, *Proc. R. Soc. London A* 434 (1991) 413–417.
- [33] M.J. Lyons, L.G. Harrison, Stripe selection: an intrinsic property of some pattern-forming models with nonlinear dynamics, *Dev. Dyn.* 195 (1992) 201–215.
- [34] A.J. Perumpanani, J.A. Sherratt, P.K. Maini, Phase differences in reaction-diffusion-advection systems and applications to morphogenesis, *IMA J. Appl. Math.* 55 (1995) 19–33.
- [35] M.A. Russell, Positional information in insect segments, *Dev. Biol.* 108 (1985) 269–283.
- [36] P. Arcuri, J.D. Murray, Pattern sensitivity to boundary and initial conditions in reaction-diffusion equations, *J. Math. Biol.* 24 (1986) 141–165.
- [37] R.A. Satnoianu, M. Menzinger, P.K. Maini, The universal principle of flow and diffusion distributed structures, in preparation.

- [38] M. Kaern, M. Menzinger, R.A. Satnoianu, A. Hunding, Chemical waves in open flows of active media: their relevance to axial segmentation in biology. Faraday Discussions, Sept. 2001, Manchester invited paper, in press.
- [39] R.A. Satnoianu, M. Menzinger, Inexact phase differences in reaction-diffusion-advection systems: Positional information and cellular calculus, submitted, 2001.
- [40] J.S. Nagumo, S. Arimoto, S. Yoshizawa, An active pulse transmission line simulating nerve axon, Proc. IRE 50 (1962) 2061–2071.
- [41] R. FitzHugh, Impulses and physiological states in theoretical models of nerve membrane, Biophys. J. 1 (1961) 445–466.
- [42] B.P. Belousov, A periodic reaction and its mechanism English translation, in: R.J. Field, M. Burger (Eds.), *Oscillations and Travelling Waves in Chemical Systems*, Wiley, New York, 1985.
- [43] A.M. Zhabotinskii, Periodic processes of the oxidation of malonic acid in solution (study of the kinetics of Belousov's reaction), Biopfizika 9 (1964) 306–311.